Aerodynamic Efficiency Study of Modern Spiroid Winglets

Tung Wan Hung-Chu Chou Kuei-Wen Lien
Department of Aerospace Engineering, Tamkang University, Taiwan, R.O.C.

Abstract

The objective of this work is to gain greater understanding of how the wing tip device modifies the vortex structure. Use ATR-72 wing as the datum; add different types of winglet shape at Mach number 0.2 and 0.41, to compare the differences in C_L and C_D. Besides a new winglet appearance - spiroid winglet, we also design different kinds of spiroid winglet, including spiroid winglets with different cant angles, different sprial radius, and cambered winglet airfoil. It is hoped to find optimal shaped winglet in order to achieve the aerodynamic performance and fuel-efficient goals.
Keywords: Spiroid Winglet

1. Introduction

In last thirty years, wingtip devices have aroused aerodynamicist's attention in order to improve modern aircraft's performance. As aircraft get larger and fly farther, the payoff in wingtip devices technology will be more dramatic. For example, a Boeing 747, enhanced with Aviation Partners Technology proposed winglet, would save an estimated 23,000 pounds of fuel on flights form U.S. West Coast to Hong Kong. At typical utilization rates, this could translate into saving of more than a million gallons of fuel a year per aircraft. Alternative, one could fly approximately an hour farther across the Pacific or carry additional payload [1].

The problem of aerodynamics of wingtip region and wingtip devices arises when studying ways of increasing aerodynamic efficiency. Important advantage of using wingtip devices as additional aerodynamic means is the fact that it can be mounted on existing aircraft without serious wing structure modifications. At the same time it can be considered as alternatives to wing extensions made for enhancing the lift-to-drag ratio both in aircraft design and in improving existing aircraft [2]. However, the effectiveness of wing with various wingtip devices is substantially dependent on flight regime parameters such as Mach number, Reynolds number, angle of attack, etc. The purpose of this study is to focus on comparing various winglet shapes at different angles of attack and Mach numbers, and hopefully to find the optimal winglet appearance which could reduce the drag most.

2. Literature Review

Winglets are wing-like tip devices that reduce the vorticity strength of wingtip trailing vortices and thereby reducing drag. If a wing is producing lift, there must be higher pressure on the underside of the wing than on the upper side. In other words, there will be a spanwise flow on the finite wing that was not present on the infinite wing (Fig. 1). This spanwise flow is felt all along the trailing edge as the flow leaving the upper surface moves inward while that on the lower surface moves outward. As these opposing flows meet at the trailing edge, they give rise to a swirling motion that will concentrate into the two well-known tip vortices [3]. Since the energy of the vortices servers no useful purpose, this part of power is essentially lost.

A close look at the drag breakdown of a typical civil transport aircraft (Fig. 2.3), reveals that the skin friction and lift induced drag together represent more than 80% of the total drag and may offer the potential for drag reduction [4]. For a typical transport aircraft at cruise conditions, induced drag is one of the major contributors (about 35%) of the total drag [5], as shown in Fig. 2. At low speeds, the drag due to lift will constitute more of the total drag [6]. The classical way to reduce the lift-induced drag is to increase the aspect ratio of the wing. This has been done in the past and the Airbus A340 wing aspect ratio reaches 9.3. However, wing aspect ratio is a compromise between aerodynamics and structure characteristics and it is clear that for an existing airplane there is not much possibility to increase aspect ratios. The alternative is to develop wing tip devices that acting on the tip vortex, which is at the origin of the lift-induced drag.

It has been known for over a century that an endplate at the tip of finite wing can reduce spanwise flow and induced drag. Unfortunately, to be effective the endplate must be so large that the

increase in skin friction drag due to excessive wetted area far outweighs the reduction in induced drag. Winglet provides a better way-rather than being a simple "fence", it carries aerodynamic load. The idea is to produce a flow field that will interact with the main wing flow to reduce the amount of spanwise flow. That is, the spanwise induced velocities from the winglet oppose and thereby partially cancel those generated by the main wing.

In late 1960s, designers began experimenting with wing-tip geometries using 'small' vertical extensions to reduce the formation of tip vortices. But this concept actually dates back to 1897, when Frederick Lanchester took out a patent on the idea, incorporating it into some of his wing theories [7]. Richard Whitcomb essentially made the real break-through with winglets. In 1976, he published a paper on the subject that compared a high subsonic wing (0.78 Mach) with a simple extension to increase its span [8]. Whitcomb showed that winglets reduced drag by about 20 percent and increase the wing lift-drag ratio by approximate 9 percent [9]. Later, the first NASA's winglet technology applied in industry was on business jets, and winglets are now incorporated into most commercial and military transport jets, i.e., the Gulfstream Ⅲ, Ⅳ, and Ⅴ business jets, Boeing 747-400, McDonnell Douglas MD-11, C-17, and Airbus A340, A330, A310-300, and Embraer aircrafts. In recent years, many modification kits are offered for installing winglets to transport aircrafts [4].

A small company, Aviation Partners, Inc., has developed advanced winglet design for transport aircraft that could cut fuel consumption 6-10% in cruise flight. The company has been testing a new concept – Spiriod Winglets, which look like a large loop of rigid ribbon material attached to each tip. Initial flight tests of the spiriod concept on a Gulfstream II reported a reduction of cruise fuel consumption by more than 10% [1]. In this works it is the spiroid winglets that we focus our effort on.

3. Numerical Method

The software that used in this study is FLUENT, it is using quite extensively, including aircraft aerodynamics, electronics heat transfer, mobile engine thermodynamics, tunnel ventilating, combustion, etc. The grids we used is unstructured type for its simplicity, and the outer boundary is supplied by Pro-E software. To observe the characteristics of wing tip vortices, the airplane we choose is ATR-72 civil transport, and the 3-D unstructured grids for this bare wing are shown in Fig. 3. In addition, we also drew two other winglets to compare. Adding a winglet on original ATR-72 wing, the winglet shape is produced by simply extend and bend the original wing proportionally, and winglet cant angle (angle between the winglets datum plane and vertical plane) is about 30 degrees [Fig.4]. As shown in Fig. 5, the other one is spiroid winglet and it is a spiral loop when a vertical winglet (front) and a horizontal one (rear) joined at their tips.

For all flows, FLUENT solves conservation equations of mass and momentum. The equation for conservation of mass, or continuity equation, can be written as follows:

$$\frac{\partial \rho}{\partial t} + \nabla \bullet \left(\rho \vec{v} \right) = 0 \qquad (1)$$

Conservation of momentum is described by

$$\frac{\partial}{\partial t}\left(\rho \vec{v} \right) + \nabla \bullet \left(\rho \vec{v} \vec{v} \right) = -\nabla p + \nabla \bullet \left(\bar{\bar{\tau}} \right) + \rho \vec{g} \quad (2)$$

The stress tensor $\bar{\bar{\tau}}$ is given by

$$\bar{\bar{\tau}} = \mu \left[\left(\nabla \vec{v} + \nabla \vec{v}^{T} \right) - \tfrac{2}{3} \nabla \vec{v} I \right] \qquad (3)$$

where μ is the molecular viscosity, I is the unit tensor.

The Reynolds-averaged Navier-Stokes (RANS) equations represent transport equations for the mean flow only, with all turbulence scales being modeled. Generally, this Reynolds-averaged approach is adopted for many practical engineering calculations, and uses models such as Spalart-Allmaras, $k-\varepsilon$ and its variants, $k-\omega$ and its variants, etc. With the usual Boussinesq hypothesis, it is the Reynolds-averaged Navier-Stokes equations implemented with turbulence models that we choose for our simulation.

To test the validity of our computation, first an NACA0012 airfoil [10] is considered and its flow field is solved. The result is that using k-ε model in N-S equation is more accurate. The error between our calculation and existing experimental value of Cl value is smaller than 3%, thus give us some confidence. In order to validate the accuracy of computational results of different grid density, boundary type, and turbulence model, a benchmark case also needs to consider. The test case is the standard three-dimensional ONERA M6 wing [11]. It is a swept, semi-span wing with no twist. The coordinates of the airfoil section at the (y/b) = 0.0 plane are listed in the Schmitt and Charpin report [14]. Comparison data consists of pressure

coefficients at sections along the wingspan obtained in the experiment by Schmitt and Charpin, and computational data by J.W. Slater. In addition, we must verify that whether the drag coefficient calculated by FLUENT included frictional drag. A flat plate is drawn and its drag is calculated to compare with the Blasius solution for laminar flow. The drag coefficient of the flat plate solved by Blasius is

$$Cd = \frac{1.328}{\sqrt{\mathrm{Re}}}$$

This equation is about 0.0507, and FLUENT calculation is about 0.0464, difference between the two is about 8.53%, within acceptable tolerance and justify that Fluent do include the frictional drag.

4. Results and Discussion

The cases we considered including seven angles of attack, which are 0, 2, 4, 7, 10, 13 and 16 degrees. ATR-72 maximum cruising speed is set as 0.41 Mach. Fig. 6 to 8 are showing the wing pressure distribution at M=0.41 cruise condition. After adding winglet, the tip vortices will be different from that of a bare wing. In addition to the original primary vortex of bare wing, now two secondary tip vortices exist, located at the main wing tip and winglet tip. Furthermore, it should be noted that the intensity of the winglet tip vortex is much weaker than that of the bare wing. However, for spiroid winglet the situation is different. Now the tip vortex produced by spiroid winglet is spreading wider, and the intensity of this vortex is also weaker than the vortex produced by simple winglet.

Besides velocity vectors, pathlines is another tool to visualize the flow field. By Fig. 9, it can be shown that when pathlines passing the adjacent bare wing tip, pressure difference between upper and lower surface will push the air and causing a whirling motion. Fig. 10 to 12 showed the vorticity contour of three different winglets. It was shown that near the wing tip the vorticity is strongest in the bare wing case. After adding the simple winglet, vorticity spreads to the vicinity of winglet tip, and strength is decreased. For spiroid winglet, vorticity is further diffused, and strength is much less than the last two.

In addition, in order to find the optimal shaped spiroid, we have also drawn four more types of spiroid winglet, including the spiroid winglet's cant angle equal to 45 and 15 degrees (Fig. 13 and 14)(the original spiroid winglet's cant angle is about 30.4 degree), and the third one is with increased spiroid's radius (Fig. 15). So far these spiroid winglets' airfoils are all NACA0012 airfoils, but the last spiroid winglet's airfoil is ATR-72 cambered airfoil. Compare with the original spiroid winglet, in Tables listed C_L and C_D values of bare wing and wing with various types of winglet under different angles of attack. Obvious C_L values of bare wing are minima, and C_D values are maxima. After adding the simple winglet, lift is increased and drag decreased, so it is helpful in improving aircraft's performance and saving fuel.

Changing to spiroid winglet, drag will decrease more. With increasing angle of attack, the induced drag is proportional increasing, and the percentage of the decreasing drag from winglet is increasing, too. Although the percentage of C_L increases is diminished, however, in the cruising condition, there is plenty of lift and we care more about the drag because it directly related to how much fuel we can save. When spiroid winglet's cant angle equal to 45°, its shape is more like when the wing extending its span. Also, the characteristic of this spiroid winglet is not obvious, now lift is increasing, but the reduction of drag is less. Moreover, when spiroid winglet's cant angle equals to 15°, drag coefficient is close to the original spiroid winglet, and lift coefficient is smaller than the original one. It represents that the reducing induced drag ability of this new spiroid is nearly same as the original, but its profile drag is increased. As angle of attack increase, induced drag is increase, too, and C_D percentage differences between this 15° spiroid winglet and the original spiroid is reduced. The other, when radius of spiroid increases, wetted area becomes larger, so drag becomes larger accordingly. It can be shown that when angle of attack more than 7°, induced drag has taken the majority, and C_D value of larger radius spiroid winglet is smaller than the spiroid with 45° cant angle. It means that the reducing induced drag ability of larger radius spiroid winglet is better than the spiroid with 45° cant angle. Table is also showing L/D values of bare wing and wing with various winglet shapes at 0.41 and 0.2 Mach. Clearly at the same angle of attack, L/D values at M=0.41 are more than that at M=0.2, so it will be more beneficial to fly at this faster speed.

Without aircraft manufacturers' help, the above ATR-72 different winglet shapes are created to the best of our knowledge, and the resulting lift, drag coefficients, and lift-to-drag ratio are all seem to be surprising satisfactory. Among them the

original spiroid winglet with 30.4° cant angle give the best efficiency. Thus it is proved that the usages of spiroid winglet will indeed enhancing the transport aircraft's performance.

5. Conclusion

Effect of different winglet shapes (including simple and spiroid winglets) on tip vortices has been computationally investigated. The results included C_L and C_D at various angles of attack with different winglet shapes, flow visualization over the wing surface. Tip vortices formed by different winglet shapes are different from each other, and C_L and C_D values differ form each other, too, indicating the winglet's effect on induced drag. Furthermore, winglets displace the primary tip vortex and changed its shape in comparison with that of the bare wing, and these primary vortices differ for each winglet. Although original simple winglet and modern spiroid winglet are all for high subsonic aircraft, but our simulated ATR-72 at 0.41 Mach and below calculations still proved that it is beneficial to implement spiroid winglet at these speede. Thus the information gained in this study may lead to the optimal design shape of modern spiroid winglet.

In this study we successful simulate trailing vortices with FLUENT. But until now real wing's 3-D configurations are still considered as industrial secrets by most aircraft manufacturers. In the future it is hoped to acquire more truly airplane's 3-D wing data, so more realistic spiroid winglet computations can be performed. Finally, as the new energy crisis is right at the corner and air transportation efficiency is becoming more important, and from the limited calculations done here, it is strongly recommended the use of spiroid winglet on future medium and long range transport aircrafts.

References

[1] The Spiriod-Tipped Wing, 2001, available on-line;
URL:http://www.aviationpartners.com/company/concepts.html

[2] Kravchenko, S.A., "The Application of the Wing Tip Lifting Surfaces for Practical Aerodynamic", Proceeding of the 20th ICAS, Napoli, Italy, 1996, Vol. 20/V2.

[3] Maughmer, Mark D., "About Winglets", available on-line;
URL:http://www.mandhsoaring.com/articles/WL-Soaring.pdf

[4] Mohammad, Reza Soltani, Kaveh Ghorbanian, and Mehdi Nazarinia, "Experimental Investigation of the Effect of Various Winglet Shapes on the Total Pressure Distribution Behind a Wing", Proceeding of the 24th ICAS, Yokohama, Japan, 2004.

[5] Thiede, P., "Aerodynamic Drag Reduction Technologies ", Proceedings of the CEAS/Drag Net European Drag Reduction Conference, 19-21 June 2000, Potsdam, Germany, 1st Ed., Springer, 2001.

[6] Kroo, I., "Drag Due to Lift: Concepts for Prediction and Reduction", Annual Review of Fluid Mechanics, Vol. 333, pp. 587-617, 2001.

[7] Lanchester, F W., "Aerodynamics", Constable & Co, London, 1907.

[8] Whitcomb, R T., "A Design Approach and Selected Wing-Tunnel
Result at High Subsonic Speed for Wing-Tip Mounted Winglets" NASA TN D-8260, July 1976.

[9] Anderle, P., F.N. Coton, L. Smrcek, and V. Broz, "A Wing Tunnel Based Study of the Flow Field Behind Sailplane Winglets", Proceeding of the 24th ICAS, Yokohama, Japan, 2004.

[10] Abbott, I., and A. Von Doenhoff, "Theory of Wing Sections: Including a Summary of Airfoil Data", New York, Dover Publications, 1959.

[11] The ONERA M6 Wing, available on-line;
URL:http://www.grc.nasa.gov/WWW/wind/valid/m6wing/m6wing01/m6wing01.html

[12] The ONERA M6 Wing, available on-line;
URL:http://www.grc.nasa.gov/WWW/wind/valid/m6wing/page07.pdf

[13] Catalano, F.M., H.D. Ceron-Munoz, "Experimental Analysis of Aerodynamics Characteristics of Adaptative Multi-Winglets", Proceeding of the 24th ICAS, Yokohama, Japan, 2004.

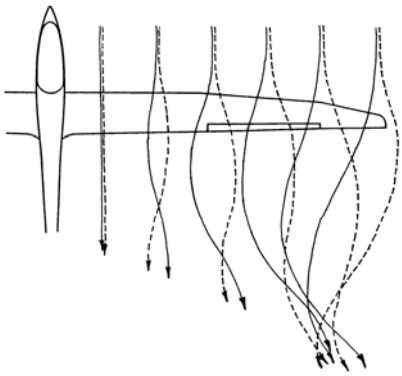

Figure 1. Spanwise flow on a finite wing–solid, upper surface; dashed, lower surface [3]

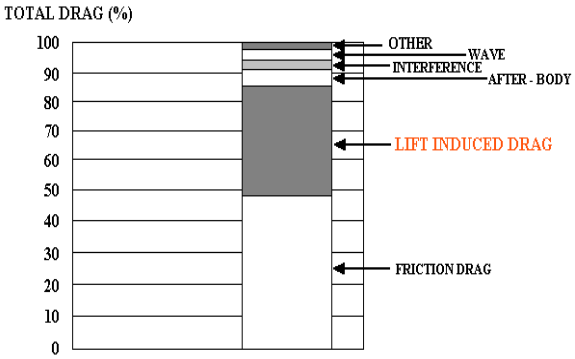

Figure 2. Drag breakdown of a typical transport aircraft [5]

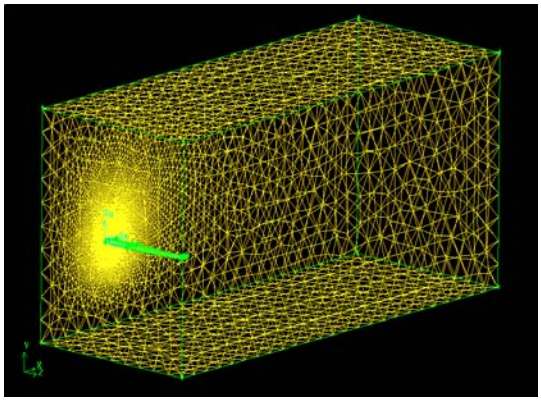

Figure 3. 3-D unstructured grids

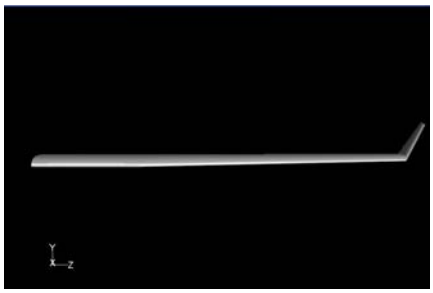

Figure 4. 3-D wing with winglet model

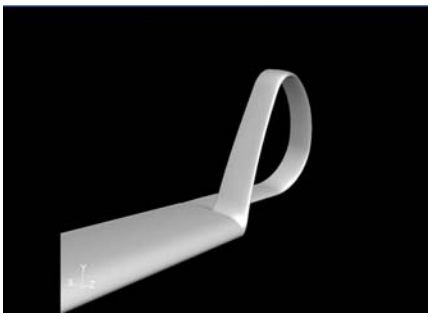

Figure 5. 3-D wing with spiroid winglet model

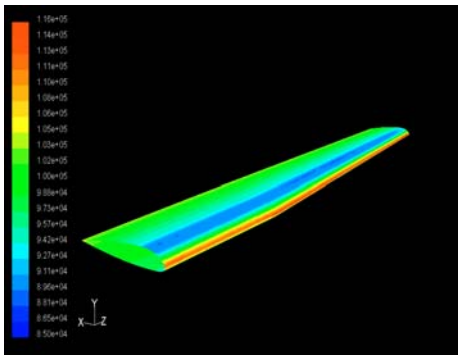

Figure 6. Pressure distribution on bare wing

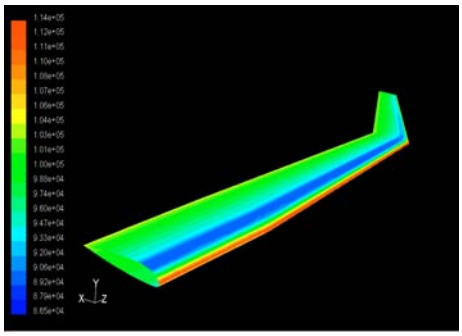

Figure 7. Pressure distribution on wing with winglet

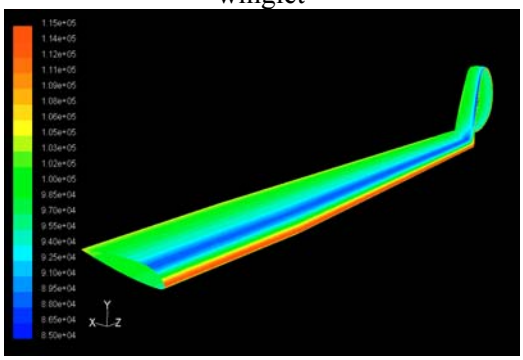

Figure 8. Pressure distribution on wing with spiroid winglet

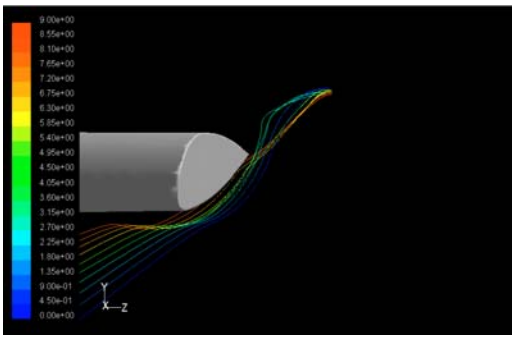

Figure 9. Pathlines at wingtip

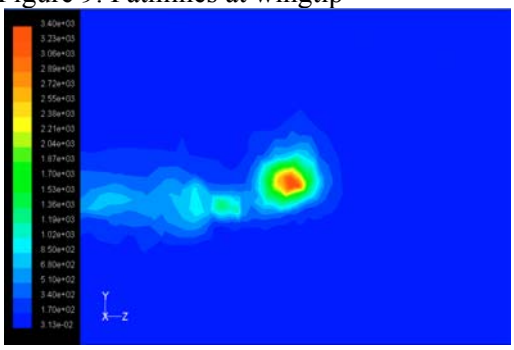

Figure 10. Vorticity contour of bare wing

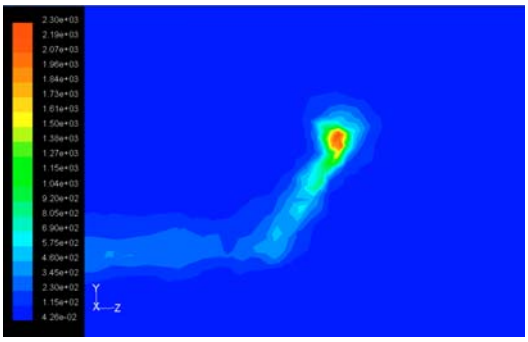

Figure 11. Vorticity contour of wing with winglet

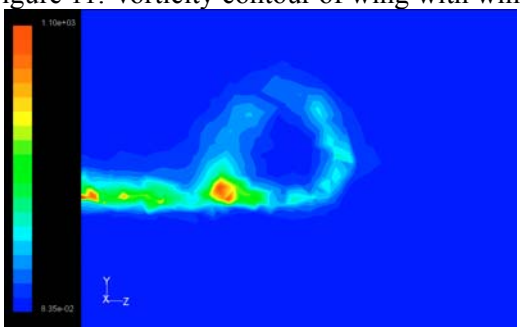

Figure 12. Vorticity contour of wing with spiroid winglet

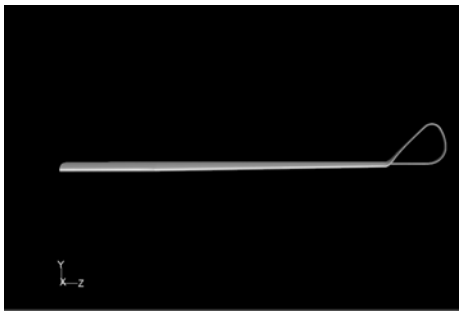

Figure 13. Wing and spiroid winglet with cant angle=45◦

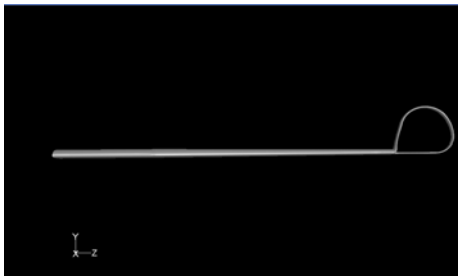

Figure 14. Wing and spiroid winglet with cant angle=15◦

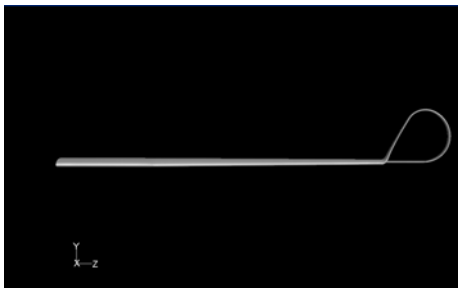

Figure 15. Wing and spiroid winglet with larger radius

α / Shapes	0◦	2◦	4◦	7◦	10◦	13◦	16◦
Wing	0.026709 0.197959 7.411811 6.687446	0.029769 0.407376 13.684805 12.490780	0.038929 0.606879 15.589210 14.618769	0.061708 0.885808 14.354787 13.954323	0.095149 1.143554 12.018534 11.861124	0.138306 1.353947 9.789536 9.837820	0.189349 1.483350 7.833938 7.943594
Wing + simple winglet	0.026670 0.208566 7.820135 7.040195	0.029674 0.421362 14.199570 12.900521	0.038720 0.622047 16.065480 15.048785	0.061265 0.910798 14.866571 14.353368	0.094136 1.170745 12.433668 12.179538	0.137747 1.380826 10.024356 10.066953	0.188198 1.516322 8.057063 8.161452
Wing + Spiroid winglet	0.026481 0.213313 8.055375 7.283985	0.029381 0.428310 14.577539 13.194564	0.038210 0.628747 16.455258 15.348246	0.060182 0.914724 15.199332 14.692977	0.09204 1.173776 12.752373 12.500742	0.136412 1.384846 10.151913 10.350151	0.186616 1.520350 8.146965 8.444707
Wing + Spiroid winglet (cant=45)	0.026542 0.214354 8.075886 7.300180	0.029464 0.430235 14.601824 13.211559	0.038325 0.631395 16.474741 15.347582	0.060431 0.918288 15.195671 14.671096	0.092619 1.179085 12.730451 12.471958	0.136840 1.389916 10.157238 10.368590	0.187229 1.525633 8.148492 8.461269
Wing + Spiroid winglet (cant=15)	0.026497 0.212506 8.020147 7.254534	0.029399 0.426915 14.521368 13.152645	0.038230 0.627129 16.404175 15.308355	0.060209 0.912805 15.160518 14.665626	0.092232 1.172019 12.707347 12.471240	0.136501 1.383372 10.134505 10.303598	0.186720 1.518866 8.134428 8.434863
Wing + Spiroid winglet (+R)	0.026554 0.213367 8.035357 7.265428	0.029480 0.428494 14.535070 13.158040	0.038367 0.628998 16.394251 15.302744	0.060422 0.915372 15.149724 14.657838	0.092568 1.174550 12.690618 12.420769	0.136725 1.385789 10.135593 10.283859	0.186920 1.521861 8.141770 8.387746
Spiroid of camberd airfoil section	0.026508 0.214011 8.073362 7.294608	0.029422 0.429611 14.601497 13.211515	0.038280 0.630325 16.466015 15.350021	0.060325 0.917065 15.202035 14.687179	0.092356 1.177623 12.75084 12.486573	0.136662 1.387864 10.155415 10.366596	0.186784 1.522278 8.149934 8.485122

Table (1^{st} value) C_D values of different wing and winglet shapes at various angles of attack for M=0.41
(2^{nd} value) C_L values of different wing and winglet shapes at various angles of attack for M=0.41
(3^{rd} value) L/D values of different wing and winglet shapes at various angles of attack for M=0.41
(4^{th} value) L/D values of different wing and winglet shapes at various angles of attack for M=0.2